Journal of Renewable and Sustainable Energy

RESEARCH ARTICLE | FEBRUARY 10 2025

Gaussian FLOWERS: Wind-rose-based analytical integration of Gaussian wake model for extremely fast AEP estimation

Special Collection: Flow, Turbulence, and Wind Energy

Caidan Whittaker ; Michael J. LoCascio ; Luis A. Martínez-Tossas ; Christopher J. Bay ; Majid Bastankhah

Check for updates

J. Renewable Sustainable Energy 17, 013306 (2025)
https://doi.org/10.1063/5.0245886
CHORUS

View Online
Export Citation

Articles You May Be Interested In

Efficient wind farm layout optimization with the FLOWERS AEP model and analytic gradients

J. Renewable Sustainable Energy (January 2025)

Monte-Carlo simulations based hub height optimization using FLORIS for two interacting onshore wind farms

J. Renewable Sustainable Energy (November 2022)

Design and implementation of wind energy analysis tool (WEATb) in Iraq

AIP Conf. Proc. (August 2019)

24 February 2025 17:31:52

AIP Publishing

Special Topics Open for Submissions

Learn More

AIP Publishing

Journal of Renewable and Sustainable Energy ARTICLE pubs.aip.org/aip/rse

Gaussian FLOWERS: Wind-rose-based analytical integration of Gaussian wake model for extremely fast AEP estimation

Cite as: J. Renewable Sustainable Energy **17**, 013306 (2025); doi: 10.1063/5.0245886
Submitted: 29 October 2024 · Accepted: 10 January 2025 ·
Published Online: 10 February 2025

View Online Export Citation CrossMark

Caidan Whittaker,[1] Michael J. LoCascio,[2] Luis A. Martínez-Tossas,[3] Christopher J. Bay,[3] and Majid Bastankhah[1,a)]

AFFILIATIONS

[1]Durham University, Durham DH1 3LE, United Kingdom
[2]Civil and Environmental Engineering, Stanford University, Stanford, California 94305, USA
[3]National Wind Technology Center, National Renewable Energy Laboratory, Golden, Colorado 80401, USA

Note: This paper is part of the Special Topic on Flow, Turbulence, and Wind Energy.
[a)]**Author to whom correspondence should be addressed:** majid.bastankhah@durham.ac.uk

ABSTRACT

A major cost in the study of wind farm layout optimization is the repeated evaluation of the annual energy production (AEP). The current approach to estimating AEP requires a large set of flow simulations to be performed that cover each discrete wind speed and direction combination contained within the wind rose, followed by a probability-weighted sum of the power production resulting from each simulation. Even with inexpensive engineering wake models, this numerical integration scheme can lead to high computational costs. In this paper, we derive an analytical formulation for estimating farm AEP across every wind direction, based on a Gaussian wake velocity model, which reduces the number of wind farm simulations to a single function evaluation. As a result, we find that the Gaussian-FLOWERS approach reduces the time for AEP calculations by more than two orders of magnitude with a small trade-off in accuracy when compared to a conventional approach. This massive reduction in computation cost is useful to reduce overall costs in wind farm layout optimization studies.

© 2025 Author(s). All article content, except where otherwise noted, is licensed under a Creative Commons Attribution (CC BY) license (https://creativecommons.org/licenses/by/4.0/). https://doi.org/10.1063/5.0245886

24 February 2025 17:31:52

I. INTRODUCTION

In commercial wind farms, turbines are typically placed six to ten rotor diameters apart (Stevens *et al.*, 2017). This relatively close proximity means there is an insufficient distance for the turbulent structures in their wakes to fully diffuse and for the induced velocity deficits to fully recover before being transported into downwind turbines. These wake interactions lead to a 10%–20% discrepancy in energy production between the leading turbines and the farm average, as observed in the generation data of utility-scale farms (Sorensen and Nielsen, 2006; Barthelmie *et al.*, 2010).

Reducing the negative effects of these wake interactions is the primary challenge of the wind farm layout optimization (WFLO) problem. The problem is recognized as computationally complex, nonlinear, and nonconvex (Herbert-Acero *et al.*, 2014; González *et al.*, 2014). Nevertheless, studies have shown that annual energy production (AEP) can be considerably increased through tailoring the layout of turbines to the expected wind conditions (Feng and Shen, 2015; Kirchner-Bossi and Porté-Agel, 2018; and Thomas *et al.*, 2019). Numerous methods have been proposed to find solutions to the WFLO problem. Azlan *et al.* (2021) provide a comprehensive review. A common feature among the methods is the repeated [on the order of thousands (Porte-Agel *et al.*, 2020)] calculation of farm AEP to evaluate candidate layouts.

The current approach to calculating AEP uses a numerical integration approach. A wind rose is constructed by sorting observations of the incident wind into I directional bins, each with a given midpoint wind direction θ_i' and frequency f_i. For each directional bin, the incident wind is further sorted into J velocity bins, with frequency f_j. A wind farm flow simulation is then performed for each direction bin i and velocity bin j. This is necessary because in the wind-orientated perspective, the geometry of the farm changes with wind direction. Farm AEP is the sum of power production calculated for each of the bins multiplied by its frequency,

© Author(s) 2025

$$AEP = 8760 \sum_I \sum_J P(\theta_i', U_0(\theta_i')_j) f_i f_j, \quad (1)$$

where P is the total power of the wind farm as a function of wind direction θ' and freestream wind speed U_0, 8760 is the number of hours in 1 year, and f_i and f_j are the frequencies of each discrete wind direction and speed bin, respectively.

The use of high-fidelity computational fluid dynamics (CFD) within layout optimization studies is currently impractical owing to the high computational cost of each simulation, the large number of simulations required to cover every bin, and the large number of iterations required for a satisfactory solution (Shakoor *et al.*, 2016; Parada *et al.*, 2017). Instead, computationally inexpensive engineering wake models are often used, which simplify the modeling of individual turbine wakes by considering only the infinite-time-average (steady-state) flow field. Using simplified equations based on the conservation of key flow quantities such as mass and momentum and assuming a discrete "top-hat" velocity deficit profile, Jensen (1983) and Frandsen *et al.* (2006) each derived widely used engineering wake models. Bastankhah and Porté-Agel (2014) replaced the discrete velocity profile with a more realistic Gaussian profile. Compared to the Jensen model, the steady-state velocity field predicted by the Gaussian model is in closer agreement with experimental (Bastankhah and Porté-Agel, 2017), LiDAR (Zhan *et al.*, 2020; Kaldellis *et al.*, 2021), and numerical (Bastankhah and Porté-Agel, 2014) findings. When used for AEP prediction, the Gaussian model shows good agreement with historical power generation data (Doekemeijer *et al.*, 2022).

To create a wind farm model, the individual wakes are combined using a superposition approach. Lissaman (1979) suggested linear superposition of velocity deficits. Later, Katic *et al.* (1987) suggested linear superposition of energy deficits. Both are used extensively in the literature and in industry (Porte-Agel *et al.*, 2020). More recently, physics-based approaches such as those suggested by Zong and Porté-Agel (2020) and Bastankhah *et al.* (2021) have demonstrated reduced error in AEP prediction, albeit with increased complexity.

Despite the use of engineering wake models, calculating AEP remains a significant computational cost; Kirchner-Bossi and Porté-Agel (2018) reported the optimization of an 80-turbine farm using the Gaussian wake model required a computation time of about 16 CPU days. An alternative approach by LoCascio *et al.* (2022) introduced a solution for AEP based on the analytical integration of the Jensen engineering wake model across wind directions. When used to predict AEP, the FLOWERS model reduced computation time by an order of magnitude compared to the numerical integration approach. However, one identified drawback of FLOWERS was a consistent discrepancy in AEP estimates on the order of 10%.

This paper builds on the FLOWERS approach to estimating AEP with an analytical integral formulation, but a Gaussian wake velocity deficit model rather than the Jensen model is used, along with an alternative approach to handling the nonlinear terms involved in the integration. There are two objectives of this study: (1) to present the derivation of the Gaussian-FLOWERS model and justify its modeling assumptions, and (2) to compare the accuracy and performance of the Gaussian-FLOWERS predictions against the (Jensen) FLOWERS model and conventional AEP models based on numerical integration. This paper is organized as follows. The derivation of the Gaussian-FLOWERS model is detailed in Sec. II. In Sec. III, the FLOWERS model and reference models are defined. Section IV details the evaluation of the Gaussian-FLOWERS model compared to two other engineering models. Section V outlines the study's takeaways.

II. AEP MODEL FORMULATION

A. Wake characteristics of an individual turbine for a single wind direction

First, we characterize the wake flow distribution for an individual turbine subject to a single wind direction. According to the Gaussian model (Bastankhah and Porté-Agel, 2014), the wake velocity deficit in the hub height plane ($z = z_h$) is given by

$$\frac{\Delta U}{U_0}(x, y, C_T(U_0)) = \left(1 - \sqrt{1 - \frac{C_T(U_0)}{8(kx + \varepsilon)^2}}\right) \exp\left(\frac{-y^2}{2(kx + \varepsilon)^2}\right), \quad (2)$$

where $U(x, y)$ is the streamwise velocity at given streamwise x and spanwise y distances from the turbine. C_T is the thrust coefficient, which is a function of the undisturbed wind velocity U_0. For instance, $C_T(U_0)$ for the IEA 10 MW turbine (Bortolotti *et al.*, 2019) used in this study is shown in Fig. 1. The wake growth rate k is typically assumed to be a function of the incoming turbulence intensity (Niayifar and Porté-Agel, 2016). Without loss of generality and to compare the performance of the newly developed Gaussian-FLOWERS to existing models, we assume that k has a constant value of 0.03 in this paper, corresponding to a typical offshore case (Bastankhah and Porté-Agel, 2014), but other values can also be used. The normalized initial wake width is shown by ε, which is estimated to be $0.2\sqrt{\beta}$, where $\beta = \left(1 + \sqrt{1 - C_T}\right) / 2\sqrt{1 - C_T}$ (Bastankhah and Porté-Agel, 2014). Equation (2) is only valid in the far-wake region where velocity deficit profiles are estimated by a Gaussian profile, and the term under the square root is positive. Expressed in polar coordinates (r, θ), Eq. (2) reads

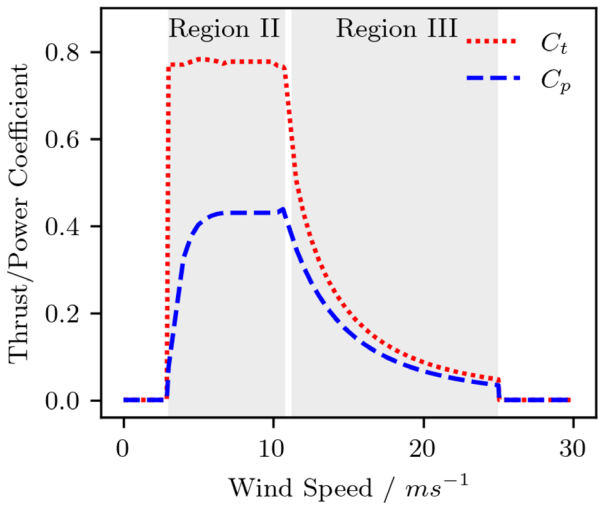

FIG. 1. Turbine thrust and power coefficient curves in different operating regions for the IEA 10 MW turbine (Bortolotti *et al.*, 2019).

24 February 2025 17:31:52

© Author(s) 2025

$$\frac{\Delta U}{U_0}(r,\theta,C_T(U_0)) = \left(1-\sqrt{1-\frac{C_T(U_0)}{8(kr\cos\theta+\varepsilon)^2}}\right) \times \exp\left(\frac{-(r\sin\theta)^2}{2(kr\cos\theta+\varepsilon)^2}\right), \quad (3)$$

where r is the normalized radial distance defined as $\sqrt{x^2+y^2}$, and $\theta = \arctan2(y,x)$ is the angle between the positive x axis and the ray from the origin to (x,y). A schematic of the coordinate system used is shown in Fig. 2(a).

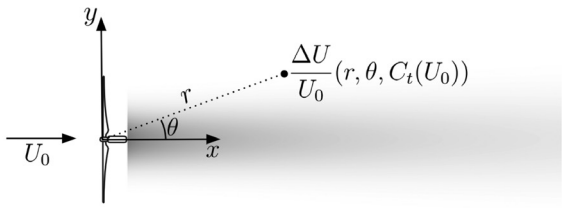

(a) Single turbine (westerly) wind direction coordinate system. Note the invalid region immediately downstream of the turbine.

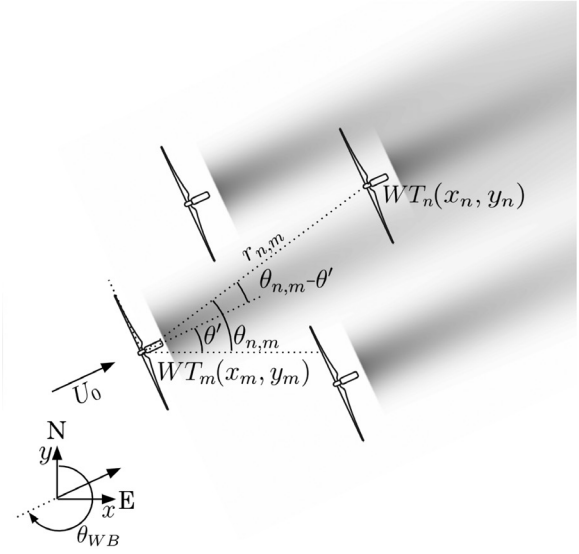

(b) Multiple turbine variable wind direction coordinate system.

FIG. 2. Coordinate systems for the flow field around a single turbine (a) and a set of turbines (b). (a) Single turbine (westerly) wind direction coordinate system. Note the invalid region immediately downstream of the turbine. (b) Multiple turbine variable wind direction coordinate system.

B. Flow distribution in a wind farm

Next, we write equations in polar coordinates for an array of turbines subject to an arbitrary wind direction. We assume the wind farm consists of N turbines where the nth turbine has coordinates (x_n, y_n) and is indicated by WT_n $(1 \le n \le N)$. We relax the assumption made earlier in Sec. II A so the origin of the coordinate system is at an arbitrary position and is no longer attached to a turbine. To maintain the linearity of the velocity-deficit equations, we use a linear superposition method (based on the global freestream inflow U_0) to account for cumulative wake effects. We allow the wind direction θ' to be variable. For each direction θ', the turbines are re-indexed from the furthest upwind ($x'_n < x'_{n+1}$ where $x'_n = x_n\cos(\theta') + y_n\sin(\theta')$). The inflow wake velocity $U_{w,n}$ for WT_n is computed by summing contributions from the other $m < n$ upwind turbines,

$$U_{w,n} = U_0\left(1-\sum_{m<n}\frac{\Delta U}{U_0}\left(r_{n,m},\theta_{n,m}-\theta',C_T(U_{w,m})\right)\right), \quad (4)$$

where $U_{w,n}$ is defined as the streamwise velocity at (x_n, y_n, z_h) if WT_n is not present, and also

$$r_{n,m} = \sqrt{(x_n-x_m)^2+(y_n-y_m)^2},$$
$$\theta_{n,m} = \arctan2(y_n-y_m, x_n-x_m).$$

Assuming x and y, respectively, denote east and north directions, $\theta' = 0$ corresponds to a (westerly) wind bearing θ_{WB} of 270° (with the turbine wakes aligned with the positive x axis). A schematic of the coordinate system used is shown in Fig. 2(b).

Total farm power generation P is found with a summation over turbines N

$$P = \sum_N \frac{1}{2}\rho A C_p(U_{w,n})U_{w,n}^3, \quad (5)$$

where $C_p(U_{w,n})$ is the power coefficient of WT_n, and for a given turbine it depends on the local flow velocity $U_{w,n}$. $C_p(U_0)$ is shown in Fig. 1. The air density is assumed to be a constant 1.225 kgm^{-3} denoted by ρ, and A is the rotor swept area.

C. Annual energy production by numerical integration

We simplify Eq. (1) by using the average wind speed per wind direction in the AEP calculation (rather than a range of wind speeds per wind direction). With this simplification, AEP is given by

$$\mathrm{AEP} \approx 8760\sum_I P(U_0(\theta'_i))f_i, \quad (6)$$

where f_i is the frequency of wind in the θ'_i direction with average wind speed U_0, and I is the total number of wind direction bins (such that $\sum_I f_i = 1$). By inserting Eqs. (4) and (5) into Eq. (6), AEP can be calculated numerically by summing the contributions of each of the discrete bins

$$\mathrm{AEP} = 4380\rho A\sum_I\sum_N C_p(U_{w,i,n})U_{0,i}^3 \times \underbrace{\left(1-\sum_{m<n}\frac{\Delta U}{U_0}\left(r_{n,m},\theta_{n,m}-\theta_i,C_T(U_{w,i,m})\right)\right)}_{\frac{U_{w,i,n}}{U_{0,i}}}{}^3 f_i. \quad (7)$$

24 February 2025 17:31:52

© Author(s) 2025

Equation (7) represents the midpoint rule numerical integration of wind farm power production over the wind direction bins (King *et al.*, 2020).

D. Annual energy production by analytical integration

1. Integral formulation

The numerical approach described in Sec. II C requires a separate simulation for each of the 72–360 wind directions (Feng and Shen, 2015) typically used in wind rose discretizations. An alternative analytical approach introduced by LoCascio *et al.* (2022) replaces the numerical integral in (7) with an analytical integral formulation. Following LoCascio *et al.* (2022), the (discrete) wind rose is defined continuously using functions $f(\theta')$ and $U_0(\theta')$ that interpolate $\frac{I}{2\pi}f_i$ and $U_{0,i}$, respectively. We calculate AEP as the solution to the integral

$$\mathrm{AEP} = 4380\rho A \int_0^{2\pi} \sum_N C_p(U_{w,n}) U_0(\theta')^3 \times \Bigg(\underbrace{1 - \sum_{m<n} \frac{\Delta U}{U_0}\left(r_{n,m}, \theta_{n,m} - \theta', C_T(U_{w,m})\right)}_{\frac{U_{w,n}}{U_0}} \Bigg)^3 f(\theta') d\theta'. \quad (8)$$

Equation (8) is a convolution using the single-direction wake model as the kernel and the wind rose as the weighting function.

2. Integral simplifications

A number of changes to Eq. (8) are needed to make the integral tractable. These simplifications will be discussed in the following, and when needed, more details on the validity of these simplifications are provided for an interested reader in the Appendixes A and B.

a. Simplification 1 - Power coefficient. For a given wind direction θ', turbines may experience lower local wind velocities due to upstream wakes, which could lead to downstream turbines operating with different power coefficients. However, for simplicity, we base the power coefficient on the undisturbed farm inflow U_0 instead of on local flow conditions $U_{w,n}$, so $C_p(U_{w,n})$ in Eq. (8) is replaced with $C_p(U_0(\theta'))$.

b. Simplification 2 - Thrust coefficient. Like C_p, the thrust coefficient C_T depends on the local velocity for each wind turbine. However, for simplicity, we use a constant value for the C_T, which we call the universal thrust coefficient $\overline{C_T}$, across all turbines and wind directions. To minimize the errors introduced by this simplification, the value of $\overline{C_T}$ is based on weight-averaging the thrust coefficient by expected power production. This ensures that $\overline{C_T}$ will be closer to the values of C_T for the directions with more frequent or stronger winds, (that have a larger contribution to AEP). Mathematically, this is defined as

$$\overline{C_T} = \sum_I f_i C_T(U_{0,i}) \frac{C_p(U_{0,i}) U_{0,i}^3}{\sum_I C_p(U_{0,i}) U_{0,i}^3}. \quad (9)$$

Also, $\varepsilon(C_T)$ in (3) is approximated with $\overline{\varepsilon} = \varepsilon(\overline{C_T})$. With the above two simplifications, Eq. (8) is approximated with

$$\mathrm{AEP} \approx 4380\rho A \int_0^{2\pi} \sum_{n=1}^{N} C_p(U_0(\theta')) U_0(\theta')^3 \times \left(1 - \sum_{m\neq n} \frac{\Delta U}{U_0}\left(r_{n,m}, \theta_{n,m} - \theta', \overline{C_T}\right)\right)^3 f(\theta') d\theta'. \quad (10)$$

Because the universal thrust coefficient is constant and does not need to be found in turn from the furthest upwind turbine, the condition on the superposition sum is changed from $m < n$ to $n \neq m$.

c. Simplification 3 - Fourier series. Similarly to LoCascio *et al.* (2022), the terms $f(\theta')C_p(U_0)U_0(\theta')^3$ in Eq. (10) are expressed using a Fourier series in cosine amplitude-phase form

$$C_p(U_0(\theta')) U_0(\theta')^3 f(\theta') = \sum_{t=0}^{T} A_t \cos(t\theta' + \phi_t), \quad (11)$$

where the term A_0 is bundled within the sum for convenience by defining $\phi_0 = 0$. Coefficients A_t and ϕ_t for the first $T \leq \mathrm{ceil}(I/2) + 1$ terms can be readily found using a discrete fast Fourier transform on the sequence $\frac{I}{2\pi}f_i C_p(U_{0,i})U_{0,i}^3$.

d. Simplification 4 - Simplifying cubic term. The term on the right-hand side of Eq. (10) is a cubic binomial, written in the form of $(1 - \sum \Delta U/U_0)^3$, which can be expanded as

$$\left(1 - \sum \frac{\Delta U}{U_0}\right)^3 = 1 - 3\left(\sum \frac{\Delta U}{U_0}\right) + 3\left(\sum \frac{\Delta U}{U_0}\right)^2 - \left(\sum \frac{\Delta U}{U_0}\right)^3. \quad (12)$$

The last term on the right-hand side of Eq. (12) is negligible given that $\Delta U/U_0$ is normally smaller than one. Moreover, we linearize $(\sum \Delta U/U_0)^2$ with the approximation $\sum (\Delta U/U_0)^2$. For most practical cases, the error introduced as a result of this simplification is fairly small. This, however, may introduce non-negligible errors for very dense wind farms or for layouts where the dominant wind direction is aligned with the turbine rows. This will be discussed in more detail in Appendix A for an extreme case and in Appendix B for more realistic operating conditions. With the two simplifications above, Eq. (10) is approximated with

$$AEP \approx 4380\rho A \sum_{n=1}^{N} \int_0^{2\pi} \left(\sum_{t=0}^{T} A_t \cos(t\theta' + \phi_t)\right) \times \left(1 - 3\sum_{m\neq n}\left(\frac{\Delta U}{U_0}\right) + 3\sum_{m\neq n}\left(\frac{\Delta U}{U_0}\right)^2\right) d\theta', \quad (13)$$

where $\frac{\Delta U}{U_0} = \frac{\Delta U}{U_0}\left(r_{n,m}, \theta_{n,m} - \theta', \overline{C_T}\right)$.

e. Simplification 5 - Gaussian wake model simplification. At typical turbine spacing distances, the velocity deficit is non-negligible only within a fairly narrow cone from the rotor axis. Therefore, a small angle approximation ($\sin\theta \approx \theta$, $\cos\theta \approx 1$) can be used to simplify the wake model in Eq. (3) to

$$\frac{\Delta U}{U_0}(r, \theta, \overline{C_T}) \approx g(r, \overline{C_T}) h(r, \theta, \overline{C_T}), \quad (14)$$

24 February 2025 17:31:52

© Author(s) 2025

where

$$g(r,\overline{C_T}) = \left(1 - \sqrt{1 - \frac{\overline{C_T}}{8(kr+\overline{\varepsilon})^2}}\right),$$

$$h(r,\theta,\overline{C_T}) = \exp\left(\frac{-1}{2}\left(\frac{m(\theta)}{\sigma_a(r)}\right)^2\right),$$

and

$$m(\theta) = \mathrm{mod}(\theta - \pi, 2\pi) - \pi, \quad \sigma_a(r) = \frac{(kr+\overline{\varepsilon})}{r}. \tag{15}$$

In Eq. (15), $\mathrm{mod}(a,b)$ is the modulo function, returning the remainder of the division of a by b. The function $m(\theta)$ wraps angle θ into the range $[-\pi, \pi]$. It is required to maintain the 2π periodicity of the wake model that is otherwise lost by using a small angle approximation. Appendix B demonstrates that this small angle approximation has a negligible impact on accuracy.

3. Integral solution

Inserting the final simplification into Eq. (13) yields a tractable integral formulation for AEP

$$AEP \approx 4380\rho A \sum_{n=1}^{N}\sum_{m\neq n}\sum_{t=0}^{T}(I_0 - 3I_1 + 3I_2), \tag{16}$$

where

$$I_\alpha = g(r_{n,m},\overline{C_T})^\alpha A_t \int_0^{2\pi} \cos(t\theta' + \phi_t) h(r_{n,m}\theta_{n,m} - \theta', \overline{C_T})^\alpha d\theta', \tag{17}$$

for $\alpha = \{0,1,2\}$. For a reasonable choice of model parameters (minimum spacing $r_{n,m} \gtrsim 3$), Eq. (17) has the solutions

$$I_\alpha = 2\pi A_0 \quad \text{for } \alpha = 0 \tag{18}$$

and

$$I_\alpha = g(r_{n,m},\overline{C_T})^\alpha \frac{\sqrt{2\pi\alpha}\sigma_a(r_{n,m})}{\alpha} \times \exp\left(-\frac{\sigma_a(r_{n,m})^2 t^2}{2\alpha}\right) A_t \cos(t\theta_{n,m} + \phi_t), \tag{19}$$

for $\alpha = \{1,2\}$. Inserting Eqs. (18) and (19) into Eq. (16) gives an analytical solution for AEP

$$AEP \approx 4380\rho A\left(2\pi A_0 + \sum_{n=1}^{N}\sum_{m\neq n}\sum_{t=0}^{T}(A_t\cos(t\theta_{n,m}+\phi_t)) \times \left(-3g(r_{n,m},\overline{C_T})\frac{\sqrt{2\pi}\sigma_a(r_{n,m})}{1}\exp\left(-\frac{\sigma_a(r_{n,m})^2 t^2}{2}\right) + 3g(r_{n,m},\overline{C_T})^2\frac{\sqrt{4\pi}\sigma_a(r_{n,m})}{2}\exp\left(-\frac{\sigma_a(r_{n,m})^2 t^2}{4}\right)\right)\right). \tag{20}$$

III. MODEL EVALUATION SETUP

A. Reference models

AEP predictions based on the Gaussian-FLOWERS formulation are compared with two other engineering wake models, summarized below.

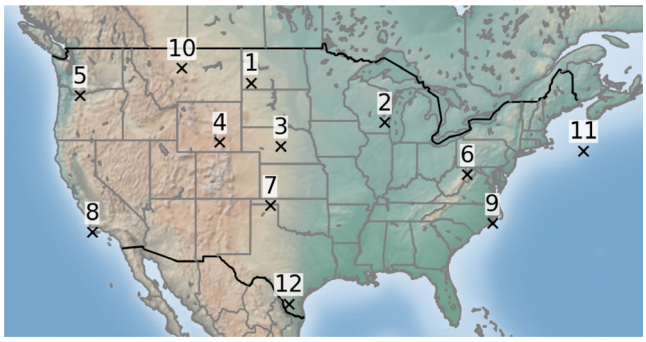

FIG. 3. Locations chosen from the Wind Toolkit dataset. The wind rose corresponding to each site is shown in Fig. 4.

1. Cumulative curl model

This model, developed by Bay *et al.* (2023) and based on the cumulative model introduced in Bastankhah *et al.* (2021), uses a Gaussian-shaped wake velocity deficit model, accounts for the effect of

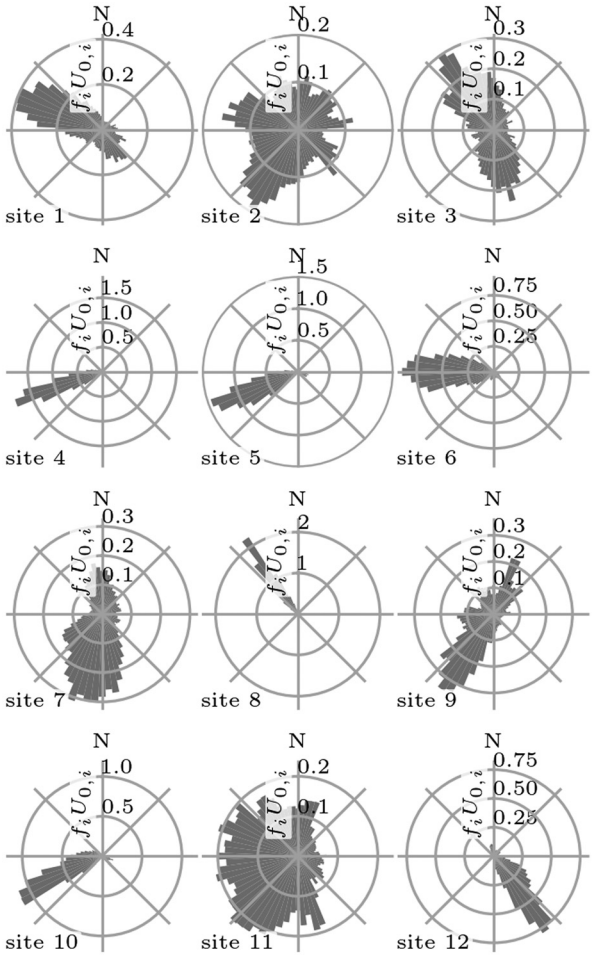

FIG. 4. Wind roses at site locations. The locations of sites are shown in Fig. 3.

24 February 2025 17:31:52

© Author(s) 2025

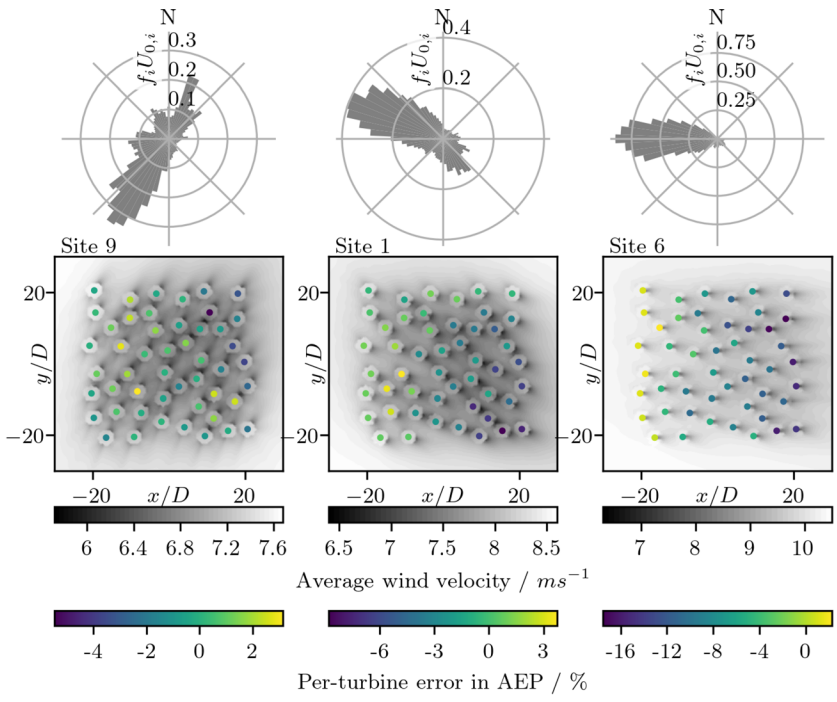

AEP			
CumulativeCurl	1303.07GWh(+0.0%)	1928.26GWh(+0.0%)	3009.22GWh(+0.0%)
GaussianFLOWERS	1301.34GWh(-0.1%)	1895.09GWh(-1.7%)	2785.92GWh(-7.4%)
JensenFLOWERS	1204.33GWh(-7.6%)	1706.37GWh(-11.5%)	3341.87GWh(+11.1%)
Performance			
CumulativeCurl	421.533ms (1.0)	426.973ms (1.0)	434.849ms (1.0)
GaussianFLOWERS	2.913ms (144.7)	2.495ms (171.1)	2.484ms (175.1)
JensenFLOWERS	6.081ms (69.3)	6.325ms (67.5)	6.374ms (68.2)

FIG. 5. Comparison of AEP prediction accuracy and performance for three example cases. The wind roses are varied over the columns of the figure, and the layout is constant. The mean velocity field surrounding the turbines is shown in grayscale. The positions of turbines are marked, and their color indicates the per-turbine percentage error of Gaussian-FLOWERS using the cumulative curl method as a reference. Percentage error and relative performance are shown in brackets also using the cumulative curl method as a reference.

wake-added turbulence in the wake recovery rate, and uses a physics-based cumulative method for the superposition of individual wakes. The added complexity of the cumulative curl model enables better predictive accuracy (Bay *et al.*, 2023), and it is currently the default wake model in the FLORIS wake modeling library (NREL, 2023). A single grid point was used to sample the wind velocity across the rotor, although FLORIS supports a two-dimensional grid of points across the rotor area. The turbulence intensity was set to 6.86%; default values were used for the remaining parameters. We would like to clarify that by comparing our model's performance with this model, we do not intend to imply that this so-called "reference" model is equivalent to the "truth." It is important to remember that the cumulative curl model is also an engineering low-fidelity model. However, this model has already been validated against high-fidelity simulations and historical data of offshore wind farms (Bay *et al.*, 2023) and is commonly used for AEP estimations and farm layout optimizations. Our goal here is to evaluate how our model compares with this state-of-the-art engineering wake model, and whether it can provide comparable AEP predictions at much lower computational costs.

2. Jensen-FLOWERS model

The original FLOWERS model developed by LoCascio *et al.* (2022) is referred to as the Jensen-FLOWERS model. This approach uses analytical integration to predict AEP but uses the top-hat wake velocity deficit model suggested by Jensen (1983). This approach uses an alternative method of linearizing the integral, where power generation is based on the weight-averaged wake velocity. Further detail is given in Appendix A. A value of 0.05 was used for the Jensen wake growth parameter, which is a commonly used value for offshore cases (Barthelmie *et al.*, 2007). Both the Jensen-FLOWERS and Gaussian-FLOWERS models are similarly implemented in vectorized Python to facilitate direct comparisons of performance.

B. Wind rose and layout generation

Twelve wind roses for use in the evaluation were generated using the WIND Toolkit dataset. The WIND Toolkit hosts publicly available annual wind forecasts at 126,000 likely wind plant sites

24 February 2025 17:31:52

© Author(s) 2025

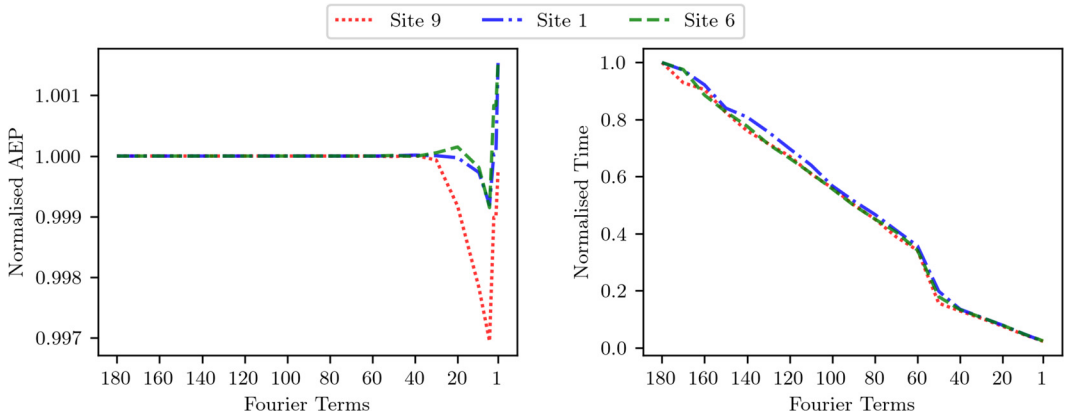

FIG. 6. Effect of varying the number of terms in the Fourier series of the wind rose on AEP accuracy and performance. Values are normalized in each plot by the 181-term value.

across the continental United States (Draxl *et al.*, 2015). The locations of the sites selected, which include both onshore and offshore cases, are shown in Fig. 3. The wind rose at each site is shown in Fig. 4. The wind data were binned using $360 \times 1^\circ$ bins and a single average wind speed per directional bin. The wind roses had minimum, average, and maximum mean wind speeds, of 7.54, 9.20, and 11.23 ms^{-1}, respectively (calculated from $\sum_I U_{0,i} f_i$). Non-uniform wind farm layouts, discussed in Sec. IV, were generated by using the Poisson disk sampling algorithm outlined in Bridson (2007) to fill a square boundary. This method produces a nonuniform set of points with a specified minimum separation.

IV. RESULTS

A. AEP accuracy: A farm layout subject to three different wind roses

We now examine the AEP prediction accuracy and performance of Gaussian-FLOWERS for three illustrative examples using a single nonuniform layout and three different wind roses.

TABLE I. Median error and variance of error for the 120 combinations of layout/wind rose combinations. Errors are computed using the cumulative curl model as a reference.

Model Name	Median AEP error	Standard deviation
Gaussian-FLOWERS	−1.59%	3.30%
Jensen-FLOWERS	−6.09%	14.17%

The nonuniform layout consists of 50 turbines positioned within a $42D \times 42D$ square boundary with a minimum separation of $5.1D$ and mean nearest neighbor distance of $6.3D$, where D is the turbine rotor diameter. This is an equivalent farm density to a $7D$ spaced rectangular grid layout (with 49 turbines placed within the same boundary).

The percentage error, hereby referred to as error, in AEP_1 using AEP_2 as a reference (i.e., cumulative curl model in this paper) is found from

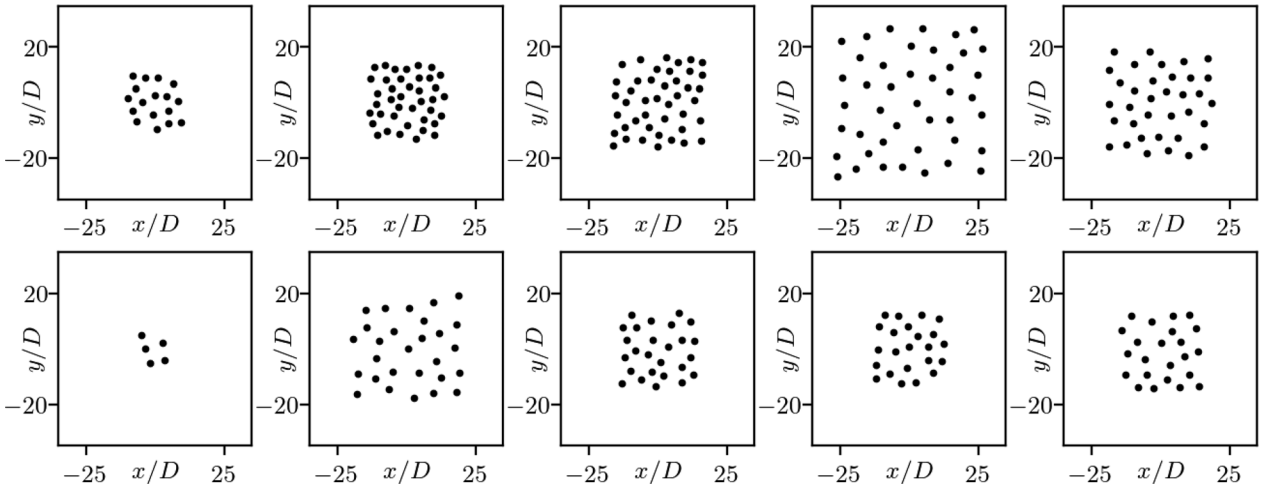

FIG. 7. Farm layouts used to evaluate the performance of the developed model in Sec. IV C. Black circles represent the location of wind turbines.

24 February 2025 17:31:52

© Author(s) 2025

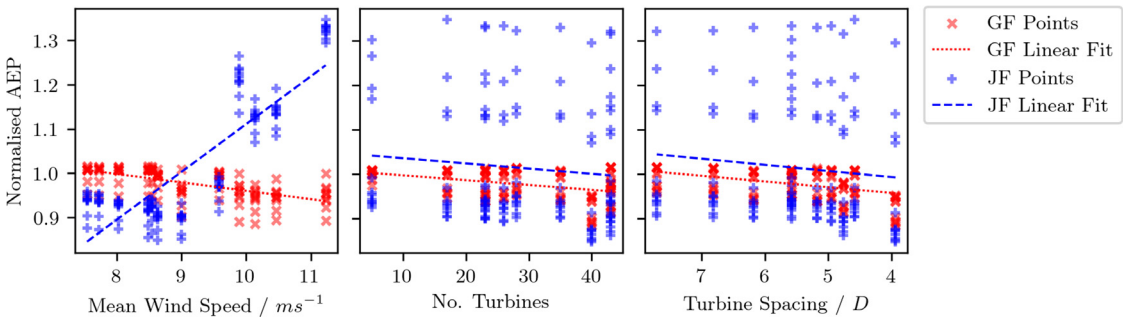

FIG. 8. Effect of wind rose and farm characteristics on AEP prediction accuracy. The predicted AEPs by Jensen-FLOWERS (JF) and Gaussian-FLOWERS (GF) are normalized by the predictions of cumulative curl model. Gaussian-FLOWERS and Jensen-FLOWERS results, as well as a linear regression, are shown in blue and orange, respectively. Turbine spacing is the mean nearest neighbor distance.

$$100 \times \frac{\mathrm{AEP}_1 - \mathrm{AEP}_2}{\mathrm{AEP}_2}. \tag{21}$$

From the complete set of 12 wind roses shown in Fig. 4, sites 9, 1, and 6 are selected for examination, chosen to cover the widest range of scenarios in terms of the performance of the Gaussian-FLOWERS model. Compared to site 9 for which the model provides the most accurate predictions, sites 1 and 6 feature more directionally concentrated winds and progressively higher average wind speeds (of 7.6, 8.5, and 10.6 ms^{-1}, respectively), which may explain the less satisfactory performance of the model in these cases. Among the twelve sites shown in Fig. 4, site 1 is the median case in terms of Gaussian-FLOWERS accuracy, while site 6 is the worst case. For these three different sites, the wind rose, farm layout, mean velocity field, farm AEP, and computational costs are presented in the left, middle, and right columns of Fig. 5.

The mean wind velocity field in Fig. 5 illustrates the impact of turbine wakes within wind farms. Turbines on the farm boundary operate undisturbed for a wide range of wind directions, while central turbines frequently experience reduced wind velocities due to upstream wakes. This results in notable variances in energy production between turbines. The largest reduction in wind speed occurs opposite the most frequent wind directions. When the wind direction is highly concentrated, the effects of turbine wakes are similarly localized. For example, for site 6, which features strongly westerly winds, the greatest reduction in wind speed is observed immediately to the east of the turbines. Figure 5 reports that for these three sites, Gaussian-FLOWERS predicts the AEP over 2 orders of magnitude faster than the cumulative curl model, with a small trade-off in the accuracy of 0.1% − 7.4%. This is an improvement on the Jensen-FLOWERS approach which achieves comparable improvement in computation time but with a larger trade-off in accuracy of 7.6% − 11.5%. The reported computation times were obtained using a single thread of an AMD Ryzen 7 3700X processor, running with 16 GB of DDR4 RAM.

The AEP of turbines that are more frequently waked are predicted with less accuracy than the leading turbines as shown in the figure. This is because simplifications 1, 2, and 4 discussed in Sec. II D 2 are less valid when there are large wake velocity deficits at the turbine locations. Although the percentage error is higher for these turbines, their contribution to AEP in absolute terms is small, so the overall accuracy is not impacted as greatly. Site 6 frequently

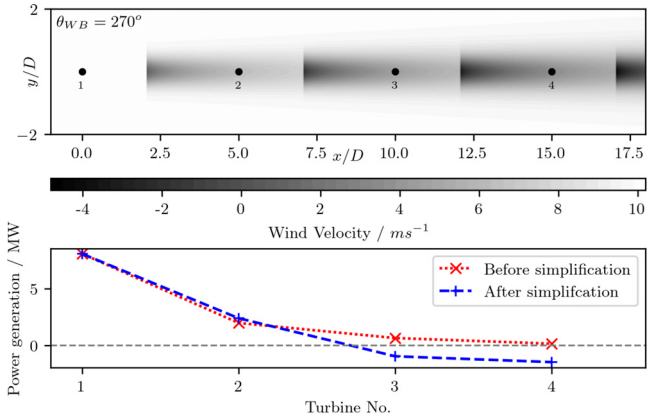

FIG. 9. Impact of simplification 4 for an extreme case of a turbine column aligned with the incoming wind direction. The upper panel shows the wind velocity, and the lower panel shows the per-turbine power generation before and after the simplification 4 outlined in Eq. (A2) for $\theta_{WB} = 270°$.

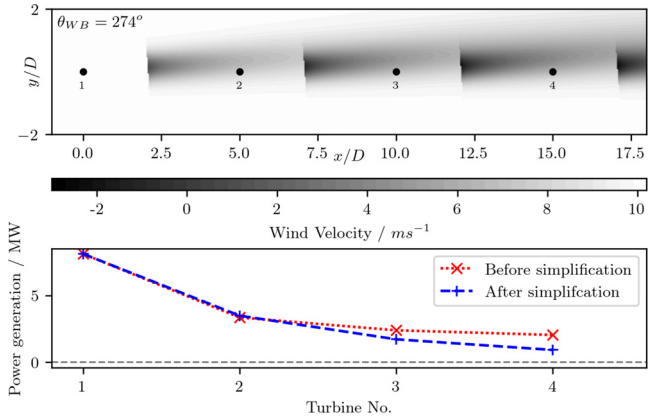

FIG. 10. Impact of simplification 4 for a turbine column with slight misalignment with the incoming wind direction. The upper panel shows the wind velocity, and the lower panel shows the per-turbine power generation before and after the simplification 4 outlined in Eq. (A2) for $\theta_{WB} = 274°$.

24 February 2025 17:31:52

© Author(s) 2025

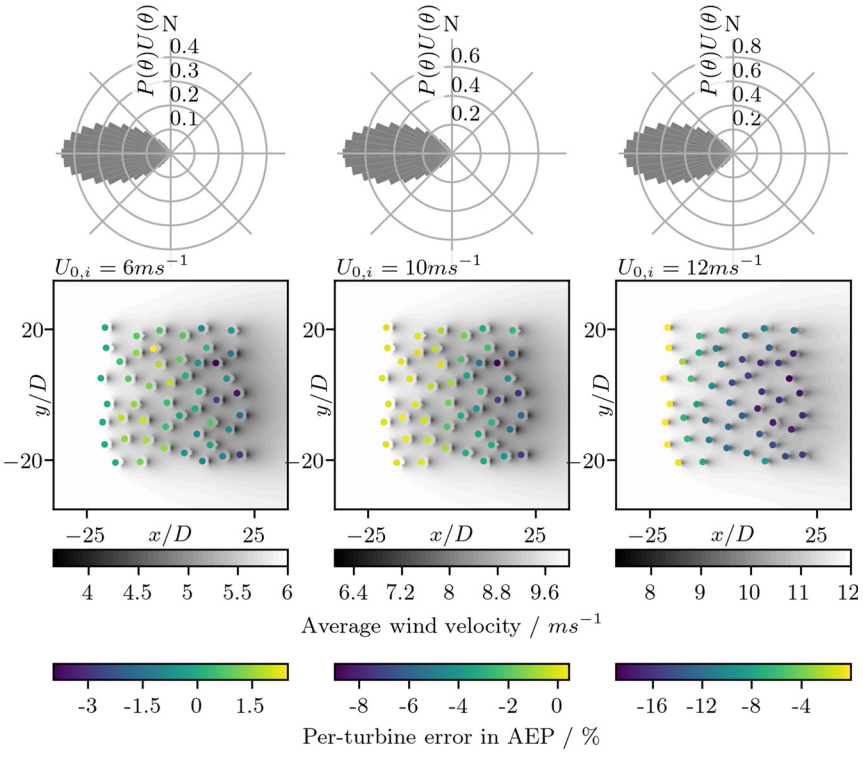

AEP			
Numerical Integration	572.17GWh(+0.0%)	2745.25GWh(+0.0%)	4144.90GWh(+0.0%)
GaussianFLOWERS	573.05GWh(+0.2%)	2691.80GWh(-1.9%)	3709.84GWh(-10.5%)
Error Contributions			
$C_t(U_w) \approx \overline{C_t}$	+0.0%	+0.0%	+1.2%
$C_p(U_w) \approx C_p(U_\infty)$	+2.2%	+0.0%	-11.2%
$(\sum x)^N \approx \sum(x^N)$	-1.8%	-2.3%	-1.1%
Sml Angle	+0.0%	+0.0%	+0.0%

FIG. 11. Comparison of AEP prediction accuracy with varying average inflow. The uniform wind speed is varied across the columns of the figure from 6, 10, and 12 ms^{-1}, left to right, respectively. The average wind velocity surrounding the turbines is shown in gray scale. The positions of turbines are marked, and their color indicates the per-turbine percentage error of Gaussian-FLOWERS using the numerical integration method as a reference. Percentage errors are shown in brackets also using the numerical integration method as a reference.

contains wind speeds above the rated speed of the turbine, where (dC_T/dU_0) and (dC_P/dU_0) are large. Assuming a constant thrust and a power coefficient based on U_0 (not U_w) is less valid, and as a result, AEP prediction accuracy diverges.

B. Computational costs

Predictions of Gaussian-FLOWERS presented in Sec. IV A were based on using the maximum number of Fourier terms (i.e., 181 terms for a wind rose with 360 bins). We now demonstrate the ability to significantly decrease the computational cost of Gaussian-FLOWERS. This is achieved by reducing the number of terms in the Fourier series representation of the wind rose, as shown in Fig. 6 for the three example cases described in Sec. IV A.

For site 1, reducing the number of Fourier terms from 181 to 10 reduces computation time by almost 18 times (from 100 times faster to 1750 times faster) but accuracy decreases by a negligible 0.03%. This speedup and sensitivity to Fourier modes is consistent with the work of LoCascio *et al.* (2022). This is enabled by the ability of the Fourier series to compactly and efficiently represent the information in the wind rose. The most important information about the wind rose is contained within the lowest frequency (higher amplitude) terms, which allows the removal of the higher-frequency terms without greatly impacting accuracy.

C. Comparison for various layout/wind rose combinations

We now examine the AEP prediction accuracy of Gaussian-FLOWERS more generally using 120 test cases generated by pairing the complete set of 12 wind roses with 10 nonuniform layouts. The number of turbines in each layout was sampled from a uniform distribution between 5 and 60 turbines, and the minimum spacing for each layout was sampled from a uniform distribution between 3.7D and 7D.

24 February 2025 17:31:52

© Author(s) 2025

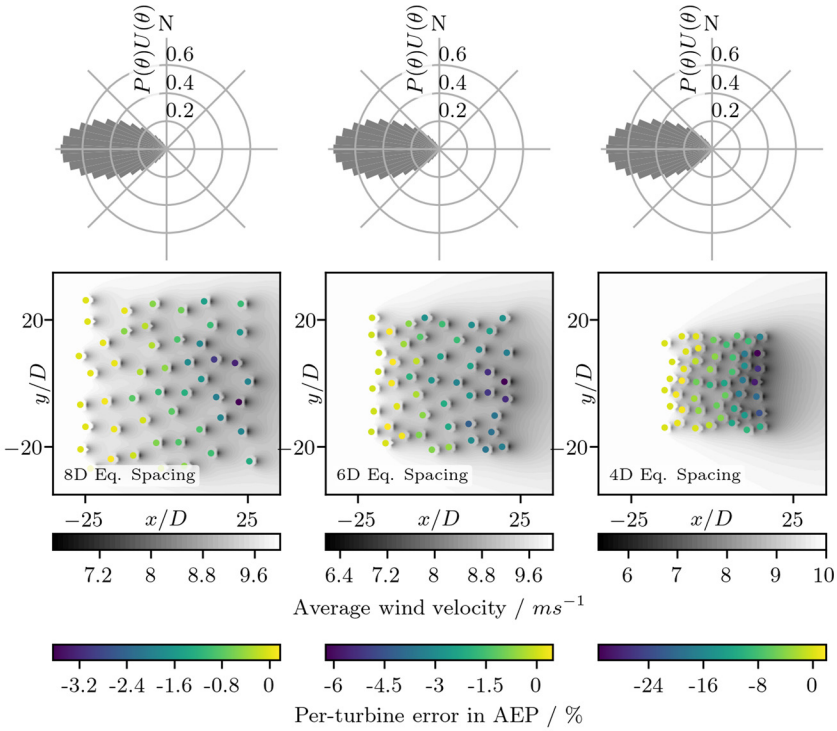

AEP			
Numerical Integration	2965.71GWh(+0.0%)	2774.01GWh(+0.0%)	2345.83GWh(+0.0%)
GaussianFLOWERS	2943.08GWh(-0.8%)	2729.35GWh(-1.6%)	2209.38GWh(-5.8%)
Error Contributions			
$C_t(U_w) \approx \overline{C_t}$	+0.0%	+0.0%	+0.0%
$C_p(U_w) \approx C_p(U_\infty)$	+0.0%	+0.0%	+0.1%
$(\sum x)^N \approx \sum(x^N)$	-0.9%	-1.9%	-6.6%
Sml Angle	+0.0%	+0.0%	+0.1%

FIG. 12. Comparison of AEP prediction accuracy with varying farm density. The layout density is varied across the columns of the figure. The average wind velocity surrounding the turbines is shown in gray scale. The positions of turbines are marked, and their color indicates the per-turbine percentage error of Gaussian-FLOWERS using the numerical integration method as a reference. Percentage errors are shown in brackets also using the numerical integration method as a reference.

This variation in density is equivalent to a regular rectangular layout with spacing between 5*D* and 9*D*, respectively. The layouts generated are shown in Fig. 7. The aggregated results for the 120 cases are shown in Table I. Over the 120 cases, Gaussian-FLOWERS predicts AEP more reliably and with greater accuracy than Jensen-FLOWERS. The Gaussian-FLOWERS approach has a lower median error of −1.59% and standard deviation of 3.30% compared to an error of −6.09% with a deviation of 14.17% of the Jensen-FLOWERS approach.

The results of the 120 cases, ordered by mean wind speed, number of turbines, and turbine spacing, are shown in Fig. 8 from left to right, respectively. A large discrepancy in accuracy between the two approaches is observed when the mean wind speed exceeds 9.5 ms^{-1}. The Jensen-FLOWERS model tends to overestimate AEP, while the Gaussian-FLOWERS model slightly underestimates. This is due to the differing methods of including the power coefficient. In Jensen-FLOWERS, the power coefficient is constant across all wind directions, based on the average wind velocity at each turbine. In Gaussian-FLOWERS, the power coefficient is variable across wind direction and is based on conditions at the farthest upwind turbine. Allowing the power coefficient to vary with directions results in more accurate power prediction when the turbine operates in Region III, which frequently occurs when the average wind speed approaches the rated speed of the turbine (11 ms^{-1} for the IEA 10MW turbine used in this study).

Increasing the number of turbines in the farm or reducing the turbine spacing decreases AEP prediction accuracy. Either action results in increased wake velocity deficits at the turbine locations due to an increased number of overlapping wakes or a reduced distance for the wake to recover, respectively. This reduces the validity of simplifications 1, 2, and 4, which assume a small wake velocity deficit. A well-optimized layout avoids large wake velocity deficits for directions that have the largest contribution to AEP. Therefore, we expect an improvement in the accuracy of AEP prediction will be observed for well-optimized layouts relative to the random layouts presented here. The dependence of the error on the wind rose and layout characteristics will be examined in more detail in Appendix B.

24 February 2025 17:31:52

© Author(s) 2025

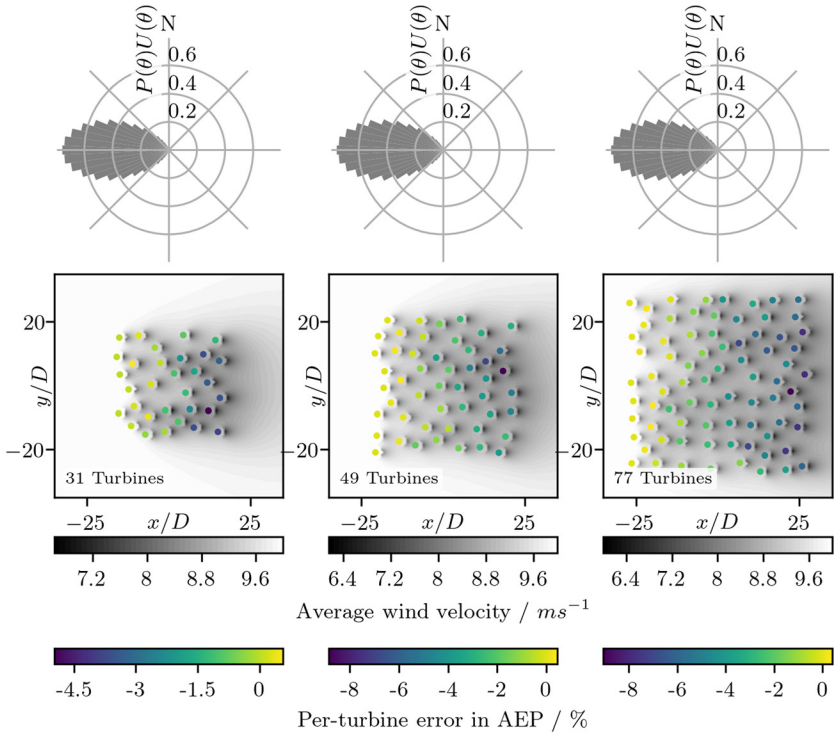

AEP			
Numerical Integration	1804.42GWh(+0.0%)	2768.35GWh(+0.0%)	4200.38GWh(+0.0%)
GaussianFLOWERS	1785.20GWh(-1.1%)	2721.15GWh(-1.7%)	4089.71GWh(-2.6%)
Error Contributions			
$C_t(U_w) \approx \overline{C_t}$	+0.0%	+0.0%	+0.0%
$C_p(U_w) \approx C_p(U_\infty)$	+0.0%	+0.0%	+0.0%
$(\sum x)^N \approx \sum(x^N)$	-1.4%	-2.0%	-3.0%
Sml Angle	+0.0%	+0.0%	+0.0%

FIG. 13. Comparison of AEP prediction accuracy with varying number of turbines. The number of turbines is varied across the columns of the figure. The average wind velocity surrounding the turbines is shown in gray scale. The positions of turbines are marked, and their color indicates the per-turbine percentage error of Gaussian-FLOWERS using the numerical integration method as a reference. Percentage errors are shown in brackets also using the numerical integration method as a reference.

V. CONCLUSION

In this paper, we derived a new engineering AEP model called Gaussian-FLOWERS. This is an analytical formulation for AEP of a wind farm using a Gaussian wake velocity deficit model, following the FLOWERS approach introduced by LoCascio *et al.* (2022). The errors introduced by our modeling assumptions, which were necessary to permit a tractable analytical integral, were characterized, and their impact on overall accuracy was shown to be small through a series of case studies. The developed model was evaluated against a current state-of-the-art engineering model and showed greater than 2 orders of magnitude performance increase with a small trade-off in accuracy. We showed the performance can further be improved by truncating the number of terms in the Fourier series, with negligible impact on accuracy. Compared to Jensen-FLOWERS, Gaussian-FLOWERS predicts farm AEP with greater accuracy, −1.59% compared to −6.09%, and with less variation, 3.30% compared to 14.17%.

Moreover, the analytical approach may provide a convenient differentiable expression if gradient-based optimization methods are used for farm layout optimization.

In general, we have demonstrated that the simplifications made in Sec. II D 2 do not typically lead to large errors in AEP estimation for most wind farms, and those simplifications were found to be necessary in order to develop an analytical formulation for the AEP. However, in certain operating conditions, these simplifications may lead to an elevated error. Future research may further explore the possibility of improving the modeling framework in the following areas:

- *Average wind velocity binning.* Modeling can be improved by describing the range of wind velocity variation within each bin rather than using an average velocity for each wind direction. For example, an alternative approach could be to integrate over a Weibull distribution whose parameters vary with direction.

24 February 2025 17:31:52

© Author(s) 2025

- *Power coefficient*. The power coefficient for each direction is set by the farthest upwind (unwaked) turbine. The possibility of using the local wind velocity can be explored.
- *Thrust coefficient*. The thrust coefficient is constant over all directions and turbine positions. Using the local wind velocity found in turn from the farthest upwind turbine can improve model predictions.
- *Nonlinear cross terms*. To linearize the integral, we neglect the "cross" terms in the expansion of $(1-\sum\frac{\Delta U}{U_0})^3$. This leads to error, and in the most extreme cases, nonphysical power generation.
- *3D effects*. We sample the wind velocity at a single point (the turbine hub centre), neglecting wind shear and variation of velocity across the swept area of the rotor.
- *Superposition method*. Linear superposition is used within the analytical framework for simplicity. More recently, physics-based approaches have shown increased accuracy.

ACKNOWLEDGMENTS

This work was authored in part by the National Renewable Energy Laboratory, operated by Alliance for Sustainable Energy, LLC, for the U.S. Department of Energy (DOE) under Contract No. DE-AC36-08GO28308. Funding provided by the U.S. Department of Energy Office of Energy Efficiency and Renewable Energy Wind Energy Technologies Office. The views expressed in the article do not necessarily represent the views of the DOE or the U.S. Government. The U.S. Government retains and the publisher, by accepting the article for publication, acknowledges that the U.S. Government retains a nonexclusive, paid-up, irrevocable, worldwide license to publish or reproduce the published form of this work, or allow others to do so, for U.S. Government purposes.

AUTHOR DECLARATIONS

Conflict of Interest

The authors have no conflicts to disclose.

Author Contributions

Caidan Whittaker: Conceptualization (equal); Investigation (equal); Methodology (equal); Visualization (equal); Writing – original draft (equal). **Michael J. LoCascio:** Conceptualization (equal); Formal analysis (equal); Investigation (equal); Methodology (equal); Writing – review & editing (equal). **Luis A. Martinez-Tossas:** Conceptualization (equal); Formal analysis (equal); Investigation (equal); Writing – review & editing (equal). **Christopher J. Bay:** Conceptualization (equal); Formal analysis (equal); Writing – review & editing (equal). **Majid Bastankhah:** Conceptualization (equal); Formal analysis (equal); Methodology (equal); Supervision (equal); Writing – review & editing (equal).

DATA AVAILABILITY

The data that support the findings of this study are available from the corresponding author upon reasonable request.

APPENDIX A: DISCUSSION ON SIMPLIFICATION 4: NEGLECTING THE VELOCITY CROSS TERMS IN AEP ESTIMATION

In Sec. II D 2, the cross terms in the expansion of $(\sum \Delta U/U_0)^2$ are neglected. Mathematically, this has the form

$$\left(\sum_N \frac{\Delta U}{U_0}\right)^2 = \sum_{n=1}^{N}\left(\frac{\Delta U}{U_0}\right)^2 + \underbrace{\sum_{n=1}^{N}\sum_{m=1}^{n-1}\left(\frac{\Delta U_n}{U_0}\right)\left(\frac{\Delta U_m}{U_0}\right)}_{\text{cross terms}} \approx \sum_N \left(\frac{\Delta U_n}{U_0}\right)^2. \tag{A1}$$

This simplification is necessary, as the number of cross terms grows combinatorially with the number of turbines—including these terms would negate the performance advantage of the analytical method.

The approximation is based on three assumptions: (i) the linear term dominates the binomial expansion so the quadratic term can be approximated without a large impact on accuracy; (ii) the wakes are narrow, so they infrequently overlap; and (iii) the wakes decay quickly, making the product of overlapping wakes negligible.

The approximation always leads to AEP underprediction because the neglected cross terms are positive. Neglecting the negative cubic term $(\sum \Delta U/U_0)^3$ partially offsets this while further reducing the computational cost. Together, the two approximations simplify the cubic binomial term in Eq. (10) to

$$\left(1-\sum\frac{\Delta U}{U_0}\right)^3 \approx 1-3\left(\sum\frac{\Delta U}{U_0}\right)+3\sum\left(\frac{\Delta U}{U_0}\right)^2. \tag{A2}$$

This was found to mainly reduce error when compared to the approach of LoCascio *et al.* (2022), which bases the power production on the weight-averaged velocity. They approximate AEP with

$$\text{AEP} \approx 4380\rho A \sum_N C_p(\overline{U_{w,n}})(\overline{U_{w,n}})^3, \tag{A3}$$

where $\overline{U_{w,n}}$ is the weight-averaged wake velocity given by

$$\overline{U_{w,n}} = \int_0^{2\pi} U_0(\theta') \times \underbrace{\left(1-\sum_{m<n}\frac{\Delta U}{U_0}\left(r_{n,m},\theta_{n,m}-\theta',C_T\left(U_0(\theta')\right)\right)\right)}_{\frac{U_{w,n}}{U_0}} f(\theta')d\theta',$$

thus avoiding the cubic binomial $(1-\sum \Delta U/U_0)^3$ term in the integral. However, in extreme cases when multiple wakes closely align, and when streamwise turbine spacing is reduced, assumptions (i) and (ii) mentioned earlier in this Appendix, respectively, are no longer valid, and this simplification can lead to nonphysical negative power contributions. Figure 9 is used to demonstrate this case. The farm layout consists of four turbines arranged in a row from east to west with a dense spacing of 5*D*. The velocity field and per-turbine power generation are shown for wind with velocity 10 ms^{-1} and direction $\theta_{WB} = 270°$ (westerly). For this wind direction, the wakes are exactly aligned with the downstream row of turbines. Before

24 February 2025 17:31:52

© Author(s) 2025

making the simplification, turbines 3 and 4 have small positive power contributions of 0.64 and 0.15 MW, respectively. After making the simplification, turbines 3 and 4 have negative power contributions of −0.97 and −1.49 MW, respectively, which are obviously nonrealistic. Changing the wind direction by only ±4° results in positive generation for all turbines. This case is shown in Fig. 10.

While this is a limitation of the Gaussian-FLOWERS approach, we argue it is unlikely to drastically affect AEP prediction accuracy in practice. For directions that have the largest contributions to AEP, and therefore the largest impact on AEP prediction accuracy, highly waked turbines are avoided by maximizing streamwise spacing and avoiding aligning wakes onto downstream turbines; for the other directions, accuracy is reduced over the narrow range of directions with aligned wakes, but these directions do not have as great a contribution to AEP.

In Appendix B, we further discuss this simplification along with other simplifications for more realistic wind farms.

APPENDIX B: ERROR CONTRIBUTIONS AND SENSITIVITY TO WIND ROSE AND LAYOUT CHARACTERISTICS FOR SIMPLIFICATIONS 1, 2, 4, AND 5

In the following, we examine the effect of varying individual characteristics of the wind rose and farm layout on the accuracy of Gaussian-FLOWERS. To identify the largest sources of error we find the error contributions of simplifications 1, 2, 4, and 5, introduced in Sec. II D 2, by solving Eq. (8) numerically. For example, AEP calculated using only the thrust coefficient simplification (i.e., simplification 2) is found by solving

$$\mathrm{AEP} = 4380\rho A \int_0^{2\pi} \sum_N C_p(U_{w,n}) U_0(\theta')^3 \times \left(1 - \sum_{m<n} \frac{\Delta U}{U_0}\left(r_{n,m}, \theta_{n,m} - \theta', \overline{C_T}\right)\right)^3 f(\theta') d\theta',$$

numerically. In the above, $C_T(U_{w,m})$ is substituted with $\overline{C_T}$ (the power coefficient, cubic binomial, and wake model are not simplified).

Assuming the error contributions are independent, the sum of the individual errors should equal the total error in Gaussian-FLOWERS (using the numerical solution as a reference). Note that simplification 3, the Fourier series representation of the wind roses, introduces negligible error and is therefore not discussed.

1. Wind velocity

We now examine the effect of varying the average inflow velocity, U_0, on the accuracy of Gaussian-FLOWERS. A single nonuniform layout and three wind roses with increasing wind velocities are used. The nonuniform layout consists of 50 turbines positioned within a $42D \times 42D$ square boundary with a minimum separation of $5.1D$. The directional frequency of the wind roses follows a von Mises distribution $M(\theta, \mu, \kappa)$, with mean direction $\mu = 0$ (westerly) and concentration parameter $\kappa = 10$. Uniform wind speeds are applied across all directions, with corresponding results depicted for three different wind speeds of 6, 10, and 12 ms^{-1} in the left, middle, and right columns of Fig. 11, respectively.

As the wind speed is increased, the error in Gaussian-FLOWERS varies from a positive value of +0.1% to a negative value of −10.4%.

The power coefficient simplification results in a positive error at 6 ms^{-1}, as $\frac{dC_p}{dU_0} > 0$ around this speed. At 10 ms^{-1}, the error is negligible as $\frac{dC_p}{dU_0} \approx 0$, and at 12 ms^{-1}, the error is negative since $\frac{dC_p}{dU_0} < 0$ around this speed.

The error from the thrust coefficient simplification is non-negligible at 12 ms^{-1} because turbines no longer operate within the constant thrust coefficient region (Region III).

The error due to neglecting the cross terms diminishes at higher wind speeds because the wakes are narrow, so they overlap less frequently. The figure also shows that the small angle approximation (abbreviated as Sml Angle in the figure) discussed in the main report as simplification 5 introduces negligible error in all cases.

2. Layout density

We now examine the effect of varying the density of the farm layout on the accuracy of Gaussian-FLOWERS. A single wind rose and three layouts are used. The directional frequency of the wind rose follows a von Mises distribution $\mathrm{M}(\theta, \mu, \kappa)$, with mean direction $\mu = 0$ (westerly), concentration parameter $\kappa = 10$, and a uniform wind speed of 10 ms^{-1} across all directions. The three nonuniform layouts consist of approximately 50 turbines positioned within a square area with side lengths of 54, 42, $32D$. This is an equivalent spacing to a 9, 7, $5.3D$ regular rectangular grid layout, respectively. Corresponding results are depicted in the left, middle, and right columns of Fig. 12, respectively.

As the farm density is increased, the error in Gaussian-FLOWERS increases from −0.8% to −5.8%. The primary source of error is the cross-terms simplification (i.e. simplification 4). With increased density, the distance for wakes to recover reduces, so the assumption that the product of overlapping wakes is negligible is less valid.

3. Farm size

We now investigate the effect of increasing the farm size on the accuracy of Gaussian-FLOWERS.

For simplicity, the directional frequency of the wind rose is determined according to a von Mises distribution $\mathrm{M}(\theta, \mu, \kappa)$ with a mean direction $\mu = 0$ and concentration parameter $\kappa = 10$. A uniform wind speed across all directions of 10 ms^{-1} was used. The three nonuniform layouts consist of 27, 48, 72 turbines positioned within a square area with side lengths of 32, 42, $54D$, respectively. As shown in Fig. 13, with an increase in the number of turbines, the error in Gaussian-FLOWERS ranges from −1.1% to −2.6%. The primary source of error is again the cross-term simplification. With increased farm size, the number of overlapping wakes deep within the farm increases, so the assumption that the product of overlapping wakes is negligible is less valid.

REFERENCES

Azlan, F., Kurnia, J., Tan, B., and Ismadi, M.-Z., "Review on optimisation methods of wind farm array under three classical wind condition problems," Renewable Sustainable Energy Rev. **135**, 110047 (2021).

24 February 2025 17:31:52

© Author(s) 2025

Barthelmie, R. J., Frandsen, S. T., Nielsen, M., Pryor, S., Rethore, P.-E., and Jørgensen, H. E., "Modelling and measurements of power losses and turbulence intensity in wind turbine wakes at middelgrunden offshore wind farm," Wind Energy **10**, 517–528 (2007).
Barthelmie, R. J., Pryor, S. C., Frandsen, S. T., Hansen, K. S., Schepers, J., Rados, K., Schlez, W., Neubert, A., Jensen, L., and Neckelmann, S., "Quantifying the impact of wind turbine wakes on power output at offshore wind farms," J. Atmos. Oceanic Technol. **27**, 1302–1317 (2010).
Bastankhah, M. and Porté-Agel, F., "A new analytical model for wind-turbine wakes," Renewable Energy **70**, 116–123 (2014).
Bastankhah, M. and Porté-Agel, F., "A new miniature wind turbine for wind tunnel experiments. part ii: Wake structure and flow dynamics," Energies **10**, 923 (2017).
Bastankhah, M., Welch, B. L., Martínez-Tossas, L. A., King, J., and Fleming, P., "Analytical solution for the cumulative wake of wind turbines in wind farms," J. Fluid Mech. **911**, A53 (2021).
Bay, C. J., Fleming, P., Doekemeijer, B., King, J., Churchfield, M., and Mudafort, R., "Addressing deep array effects and impacts to wake steering with the cumulative-curl wake model," Wind Energy Sci. **8**, 401–419 (2023).
Bortolotti, P., Tarres, H. C., Dykes, K. L., Merz, K., Sethuraman, L., Verelst, D., and Zahle, F., "IEA wind TCP task 37: Systems engineering in wind energy-WP2.1 Reference wind turbines," Technical Report (National Renewable Energy Lab.(NREL), Golden, CO, 2019).
Bridson, R., "Fast poisson disk sampling in arbitrary dimensions," in *SIGGRAPH '07: ACM SIGGRAPH 2007 Sketches* (ACM, 2007), Vol. 10, p. 22.
Doekemeijer, B. M., Simley, E., and Fleming, P., "Comparison of the gaussian wind farm model with historical data of three offshore wind farms," Energies **15**, 1964 (2022).
Draxl, C., Clifton, A., Hodge, B.-M., and McCaa, J., "The wind integration national dataset (WIND) toolkit," Appl. Energy **151**, 355–366 (2015).
Feng, J. and Shen, W. Z., "Modelling wind for wind farm layout optimization using joint distribution of wind speed and wind direction," Energies **8**, 3075–3092 (2015).
Frandsen, S., Barthelmie, R., Pryor, S., Rathmann, O., Larsen, S., Højstrup, J., and Thøgersen, M., "Analytical modelling of wind speed deficit in large offshore wind farms," Wind Energy **9**, 39–53 (2006).
González, J. S., Payán, M. B., Santos, J. M. R., and González-Longatt, F., "A review and recent developments in the optimal wind-turbine micro-siting problem," Renewable Sustainable Energy Rev. **30**, 133–144 (2014).
Herbert-Acero, J. F., Probst, O., Réthoré, P.-E., Larsen, G. C., and Castillo-Villar, K. K., "A review of methodological approaches for the design and optimization of wind farms," Energies **7**, 6930–7016 (2014).
Jensen, N. O., "A note on wind generator interaction," Technical Report Risø-M No. 2411 (Risø National Laboratory, 1983).
Kaldellis, J. K., Triantafyllou, P., and Stinis, P., "Critical evaluation of wind turbines' analytical wake models," Renewable Sustainable Energy Rev. **144**, 110991 (2021).
Katic, I., Højstrup, J., and Jensen, N., "A simple model for cluster efficiency," in European Wind Energy Conference (1987), Vol. 40.
King, R., Glaws, A., Geraci, G., and Eldred, M. S., "A probabilistic approach to estimating wind farm annual energy production with Bayesian quadrature," AIAA Paper No. 2020-1951, 2020.
Kirchner-Bossi, N. and Porté-Agel, F., "Realistic wind farm layout optimization through genetic algorithms using a gaussian wake model," Energies **11**, 3268 (2018).
Lissaman, P., "Energy effectiveness of arbitrary arrays of wind turbines," J. Energy **3**, 323–328 (1979).
LoCascio, M. J., Bay, C. J., Bastankhah, M., Barter, G. E., Fleming, P. A., and Martínez-Tossas, L. A., "Flow estimation and rose superposition (flowers): An integral approach to engineering wake models," Wind Energy Sci. **7**, 1137–1151 (2022).
Niayifar, A. and Porté-Agel, F., "Analytical modeling of wind farms: A new approach for power prediction," Energies **9**, 741 (2016).
NREL, "FLORIS: FLOw redirection and induction in steady state v3.2," https://www.nrel.gov/wind/floris.html (2023), accessed 10 November 2023.
Parada, L., Herrera, C., Flores, P., and Parada, V., "Wind farm layout optimization using a Gaussian-based wake model," Renewable Energy **107**, 531–541 (2017).
Porte-Agel, F., Bastankhah, M., and Shamsoddin, S., "Wind-turbine and wind-farm flows: A review," Boundary Layer Meteorol. **174**, 1–59 (2020).
Shakoor, R., Hassan, M. Y., Raheem, A., and Wu, Y.-K., "Wake effect modeling: A review of wind farm layout optimization using Jensen's model," Renewable Sustainable Energy Rev. **58**, 1048–1059 (2016).
Sorensen, P. and Nielsen, T., "Recalibrating wind turbine wake model parameters—validating the wake model performance for large offshore wind farms," in European Wind Energy Conference and Exhibition (EWEA) (2006).
Stevens, R. J., Hobbs, B. F., Ramos, A., and Meneveau, C., "Combining economic and fluid dynamic models to determine the optimal spacing in very large wind farms," Wind Energy **20**, 465–477 (2017).
Thomas, J. J., Annoni, J., Fleming, P. A., and Ning, A., "Comparison of wind farm layout optimization results using a simple wake model and gradient-based optimization to large eddy simulations," AIAA Paper No. 2019-0538, 2019.
Zhan, L., Letizia, S., and Iungo, G. V., "Optimal tuning of engineering wake models through lidar measurements," Wind Energy Sci. **5**, 1601–1622 (2020).
Zong, H. and Porté-Agel, F., "A momentum-conserving wake superposition method for wind farm power prediction," J. Fluid Mech. **889**, A8 (2020).

24 February 2025 17:31:52

© Author(s) 2025